Elastic-Plastic Switch of Tomato Bushy Stunt Virus Particles

A. Llauró[1], E. Coppari[2]*, F. Imperatori[3], A.R. Bizzarri[2] , L. Santi[3], S. Cannistraro[2] and P. J. de Pablo[1†].*

[1] Departamento de Física de la Materia Condensada, Universidad Autónoma de Madrid, 28049. Madrid, Spain;

[2] Biophysics and Nanoscience Centre, CNISM-DEB, Università della Tuscia, 01100. Viterbo, Italy;

[3] Department of Agriculture, Forests, Nature and Energy (DAFNE), Università della Tuscia, Via San Camillo de Lellis snc, 01100 Viterbo, Italy.

*Footnote: A. Llauró and E. Coppari contributed equally to this work.

[†]Correspondence: p.j.depablo@uam.es

The study of virus protein shells mechanics in the elastic regime has provided insights into the virus strength and structure, such as the rigidity of the shells or the precursors of the disassembly. However, there is a lack of information about the plasticity of viral cages, including their molecular and structural determinants, which results in the permanent deformation of particles without breakage. Here, we investigate the effects of pH and ions sequestration on the mechanics of individual Tomato Bushy Stunt Virus nanoparticles (TBSV-NPs) by using Atomic Force Microscopy (AFM). Our experiments show that the depletion of calcium ions from the intra-capsid binding sites reduces the stiffness of TBSV-NPs and induces an elastic-plastic transition on the mechanical response of these shells. Interestingly, we found that this plastic transition could be triggered by mechanical deformation, a fact that was also supported by a careful analysis of the virus adsorption geometries on the surface. All these results indicate that, apart from act as structural stabilizer of the capsids, calcium ions may be inextricably linked to the molecular determinants of plasticity in TBSV-NPs. Finally, we suggest that the capsid plasticity of TBSV-NPs may not only have implications during the infection of plant cells, but may also increase the stability of these cages for cargo transportation at the nanoscale.

KEYWORDS: protein shell, plasticity, RNA virus, Atomic Force Microscopy

1. INTRODUCTION

Viral capsids are self-assembled macromolecular shells that naturally protect, shuttle and release the enclosed genetic material upon the proper physicochemical conditions. [1] The stability of the viral shells has been finely tuned by evolution for responding to the variety of environmental conditions encountered along their life cycle. This enormous adaptability to the environment, together with the possibility of genetically engineering their coat protein (CP) coding sequence, have made viruses attractive systems to construct virus-derived nanoparticles (VNPs) for applications in bionanotechnology. [2] In this context, the investigation of virus physicochemical properties under different conditions has become a cornerstone for the future use of these nanostructures for human benefit. In particular, the study of virus mechanics by Atomic Force Microscopy (AFM) [3] has emerged as a powerful source of information to unravel the structural role of nucleic acids, [4, 5] mutations, [6, 7] or maturation. [8-10] Moreover, AFM has also contributed to understand the influence of environmental conditions on the stability of the viruses, including pH variations [11, 12] and humidity. [13]

The study of mechanical properties of viral shells pivots on the measurement of two parameters, the stiffness and the breaking force, both determined by recording indentation curves that result from squeezing the particles with an AFM tip. The stiffness, directly linked to the spring constant of the viral shell,[14] is obtained from the elastic regime of the deformation and permits to determine the Young's modulus of the virus on the basis of the continuum elasticity theory. [3] On the other hand, the breaking force usually corresponds to the end of the elastic regime and it is ascribed to the force needed to disrupt the capsid. [15]

However, after the elastic limit, indentation curves present a variety of nonlinearities and steps, commonly associated with the loss of structural subunits or non-linear deformations, instance that may contain relevant information about the properties of the sample. [15, 16] For example, the existence of a plastic regime in viruses, understood as a permanent deformation without fracture, has been scarcely studied. [17]

Plant virus capsids display a variety of properties particularly appropriate for their applications in nanotechnology, such as their controllable genetic manipulation, their inability to infect and replicate in vertebrates hosts, or their ease of production. [18] Tomato Bushy Stunt Virus nanoparticles (TBSV-NPs) are robust, stable, highly modifiable and easy to manufacture using *Nicotiana benthamiana* as the production host. [19] In addition, the intrinsic tendency of these viruses to form ordered aggregates has been already used to build homogeneous monolayers. [20] TBSV is a small non-enveloped virus with an outer diameter of about 33 nm and an icosahedral symmetry with a triangulation number of T=3 (Figure 1A). The viral capsid is formed by the assembly of 180 subunits of a single CP and its genome consists of a monopartite ss+RNA. [21] An additional attractive feature of TBSV-NPs is the possibility to access their inner cavity using a swelling process that mediates the reversible opening of pores on the VNPs' surface. [22] This process, which likely occurs during the first stages of the infection cycle, increases the virus dimension through a Ca^{2+}-dependent transition and is required for the release of the RNA. [23]

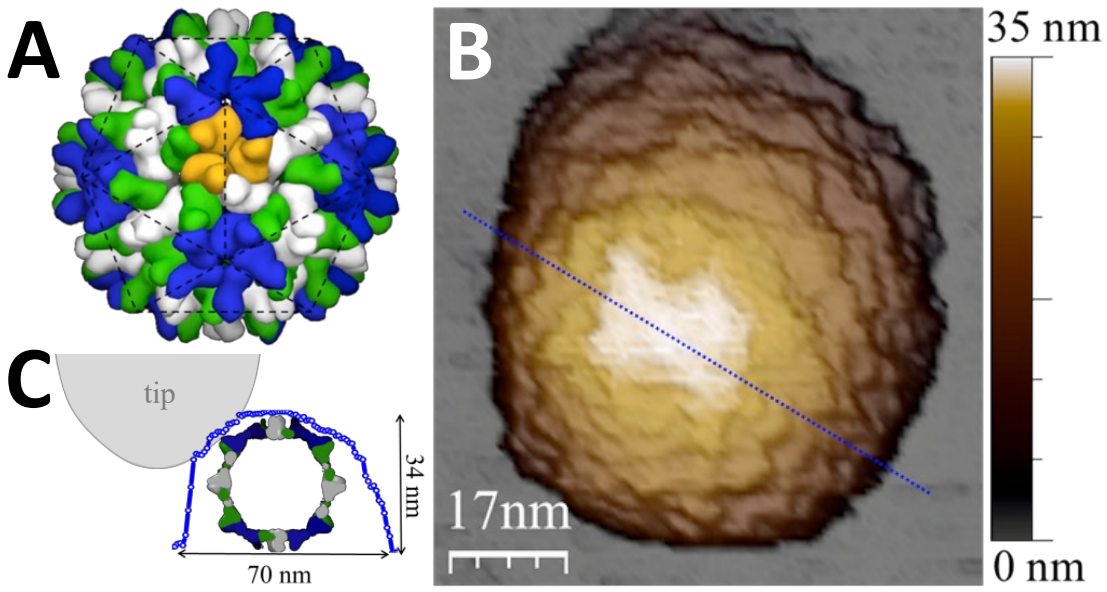

Figure 1. TBSV structure. (A) Side view derived from X-ray diffraction data *(pdb 2TBV).* [24] One of the protein trimers at the quasi-threefold axes is drawn in yellow in the structure. The trimer is composed of A-, B-, and C-type protein subunits: the A-type, packed around the 5-fold axes (blue), and the B- and C-types that alternate around the three-fold axes (colored in white and green, respectively). The black dotted lines drawn on the particle allow to extrapolate the triangulation number (T) of the virus, which describes the distribution of the capsomers on the surface of an icosahedral virus. For TBSV-NPs, T=3. (B) JM-AFM images of wt CVNPs recorded in liquid. The dotted blue shows the line along which the profile was taken. (C) Profile of the particle of B taken along its central part (dotted blue lines). Due to the dilation effect between the particle and the tip, the inserted cross section is deformed showing a broader width.

In this paper, we present the first experimental evidence of an elastic-plastic transition of individual viral particles. Our AFM images showed that under mechanical stress TBSV-NPs

were capable of deforming their structure irreversibly without fracture. In addition, we found that the intra-capsid calcium ions and mechanical deformation were, respectively, the molecular and physical determinants of virus plasticity.

2. EXPERIMENTAL DETAILS

2.1 TBSV-wt and TBSV-FLAG construct

Infectious cDNA clones were assembled using standard recombinant DNA techniques as described in details in *Grasso et al. 2012*. [19] In particular, the FLAG chimera construct is characterized by the addition at the 3' of the TBSV CP gene of an heterologous sequence encoding for a GGPGGGG protein spacer followed by the DYKDDDK FLAG sequence.

2.2 Plant infection

Six to eight weeks old *Nicotiana benthamiana* plants were inoculated with two different TBSV constructs. [19] Briefly, cDNA templates of TBSV-wt and TBSV-FLAG constructs were digested with the restriction enzyme XmaI. One μg of completely linearized cDNA was used for *in vitro* transcription reaction following the manufacturer's instructions (MEGAscript®T7 High Yield Transcription kit, Ambion Applied Biosystems). Plants were mechanically inoculated abrading the adaxial side of two leaves per plant using the carborundum powder (VWR International) mixed with the TBSV infectious RNAs, previously checked for integrity by TBE denaturing agarose gel electrophoresis.

2.3 Virus purification

Virus purification was carried out as described in Grasso *et al.* 2012. [19] Briefly, infected tissue was ground in liquid nitrogen and homogenized with 3 ml/g of ice-cold extraction

buffer [50 mM sodium acetate, 1% (w/v) ascorbic acid, pH 4.5, supplemented with a cocktail of protease inhibitors (Sigma)]. Homogenate was immediately filtered through Miracloth and, after low-speed centrifugation, the supernatant was adjusted to pH 5.0 with NaOH and ultracentrifuged for 1 h at 90000 x g at 4 °C, using a Sorvall-Thermo Scientific, WX ULTRA 100 ultracentrifuge with an AH629 rotor. The pellet was gently suspended in ice-cold acetate buffer (50 mM sodium acetate, pH 5.3) and then centrifuged at low-speed for further clarification. Quality of the preparations was verified by a silver stained 13.5% SDS-PAGE (Figure S1). Viral particles concentration was quantified using Bradford Reagent (Bio-Rad) and Bovine Serum Albumin (BSA) as reference standard.

2.4 Sample preparation for AFM measurements

We studied four different forms of TBSV-NPs: compact wt TBSV-NPs, swollen wt TBSV-NPs, recompacted wt TBSVs-NPs, and Ca^{2+}-free wt TBSV-NPs (Table 1 and Figure 2A and 2C). In addition, we investigated the FLAG chimera VNPs.

i) compact wt VNPs (wt CVNPs) and FLAG chimera VNPs: stock VNPs solution (3.03 µg/µl for wt and 8.08 µg/µl for FLAG in Na-acetate 50 mM, pH=5.3) was diluted 1:100 into the acidic buffer ($NiCl_2$ 5 mM, Na-acetate 50 mM, pH=5.3). A 20 µl drop of this diluted solution was incubated in a freshly cleaved mica surface and, after 30 minutes, washed until reaching a volume of 60 µl. The tip was also prewetted with a drop of 20 µl of the acidic buffer before starting AFM measurements. AFM images of *wt CVNPs and FLAG chimera VNP* were all conducted under acidic buffer conditions.

ii) swollen wt VNPs (SVNPs): stock virus solution was diluted 1:10 in swelling buffer (TRIS-HCl 0.1M, pH 8.5, EDTA 50 mM) and incubated for 2 hours at 4°C. Then, the solution

was diluted 1:10 in swelling buffer in the presence of $NiCl_2$ (TRIS-HCl 0.1 M, pH 8.5, EDTA 50 mM, $NiCl_2$ 5 mM) before incubating a 20 µl drop of this solution on the mica surface. After 30 minutes the sample was washed with swelling buffer, maintaining always an aqueous environment. The tip was prewetted with a 20 µl drop of swelling buffer, in which the measurements were carried out.

iii) recompacted wt VNPs (RVNPs): the swollen VNPs (stock viruses diluted 1:10 in swelling buffer during 2 hours at 4ºC) were diluted 1:10 into compacting buffer (200 mM $CaCl_2$, 50 mM Na-acetate, pH=5.3) and incubated for 2 hours at 4ºC. Afterwards, the solution was diluted 1:2 into acidic buffer and a 20 µl drop of this solution placed on a cleaved mica surface. After 30 minutes the sample was washed with the acidic buffer in which AFM images were acquired.

ii) Ca^{2+}-free wt VNPs (IFVNPs): stock virus solution was diluted 1:10 in the swelling buffer (TRIS-HCl 0.1 M, pH 8.5, EDTA 50 mM) and incubated for 2 hours at 4°C. Afterwards, the solution was 1:10 diluted into acidic buffer. A 20 µl drop of this diluted solution was deposited on a freshly cleaved mica surface and washed with acidic buffer after 30 minutes of incubation. The swelling buffer promoted the deprotonation of the aspartate residues of the calcium binding sites (pH=8.5) and the consecutive sequestration of the Ca^{2+} ions by the EDTA which, in this case, were not added when lowering the pH conditions. All the experiments were conducted under acidic buffer conditions.

2.5 AFM experiments

All measurements were conducted with an AFM (Nanotec Electrónica S.L., Madrid, Spain) operated in jumping mode plus (JM) in liquid.[25] AFM images and nanoindentation

measurements were carried out by using silicon-nitride, rectangular cantilever (Olympus, RC800PSA) with a nominal spring constant of 0.7 N/m and a tip radius of about 15 nm. We chose these cantilevers because their spring constant was similar to the spring constant of the sample, which increases the sensibility of the measurements. To calibrate the spring constant of the cantilever we used the Sader's Method.

AFM topography images were acquired in JM plus. In this mode the tip perform a force vs. distance curve (FDCs) over all the points of the image up to a given maximum force determined by the user. The tip moves from one point to another when is far from the sample, thus reducing any damage of the sample due to lateral force. Our AFM images were taken at an average controlled constant force of about 200 pN. To process the images we used the commercial software provided by WSxM.

To carry out the nanoindentation experimetns, individual FDCs were performed on top of each particle by extending the Z-piezoelectric while registering the deflection of the cantilever. All FDCs were all performed at the same z-piezo displacement (of about 17 nm from the contact point) with a loading rate of around 60 nm/s. To obtain the mechanical response of the virus, we constructed the force *vs.* indentation curve (FIC) by subtracting the piezo displacement on the particle from the piezo displacement on the substrate. [3] Then, the spring constant of the particle was obtained from the slope of the initial linear part of the FIC (green dashed lines in Figure 3A). The linear part of the indentation (regarding the elastic response of the shell) is sometimes preceded by a short-range non-linear region due to electrostatic, van der Waals, and hydration forces.[26, 27] Therefore, this initial curvature was excluded from the fitting. Likewise, the fitting was usually extends to the elastic limit.

However, if the FIC presented a shoulder before the elastic limit (as it does in the case of Figure 3C) the fitting was end before it. In these cases, the slope of the FIC after the shoulder was checked to ensure that it may be ascribed to an adjustment of the tip on the shell and not to a damage of the particle. This procedure has been established during the last decade for study of virus mechanics, some reviews have recently published the main goals achieved on this field.[14, 28] The elastic limit was considered as the maximum force reached at the end of the linear deformation. [15] During the first 5 deformations, the VNP was imaged before and after each FDC. From there on, the particle was cyclically loaded and images were taken after sets of 5 FICs. We stopped the loading when the particle responded as a solid object. All the images were analyzed using the program WSxM; [29] and the profile along the top of the VNP was taken with a 5 nm radius of influence.

3. RESULTS

3.1 Topographic characterization. The high-resolution AFM image of a typical wt CVNP on mica (Figure 1B) presents a diameter (height) fully compatible with the nominal size obtained from the X-ray structure,[24] where data from hundreds of different particles are averaged. The granular structure observed in this image can be attributed to the protruding domains present on the outer shell of the TBVV-NP. Therefore, despite the tip-particle lateral convolution (Figure 1B) we are able to achieve resolution of the order of 5 nm, which correspond to the size of the protein protrusion. To confirm that this rough appearance of the outer shell was not and artifact we confirm that the same topography was found on particles imaged with other tips (Figure S2).

In order to study the stability of the virus upon absorption, we imaged larger areas (of about 1 μm^2) under different chemical conditions and measured the height of individual particles

(Figure 2C). The statistical analysis of AFM topographies unveils that wt CVNPs and RVNPs present the same average height (red and blue bars in Figure 2E). In contrast, SVNPs collapse into structures with an average height of about 10 nm (black bars in Figure 2E). We also studied the effect of removing ions from the viral shell by decreasing the pH of SVNPs in the absence of Ca^{2+} ions. In this case, most of IFVNPs maintain their virus-like structure, with an average height of about 30 nm (green bar in Figure 2E), though the existence of structural virus subunits on the mica suggests that some of them were most likely destroyed during the adsorption (Figure 2C). This increase of small structures on the substrate for the cases of SVNPs and IFVNPs supports the idea that these two forms are the feebles, thus easier to be destroyed. To explore the instability of the virus on other substrate, we incubated the SVNPs on HOPG (Highly Oriented Pyrolytic Graphite). In this case, we found that under alkaline conditions SVNPs were disrupted in a more dramatic way than on mica (Figure S3): particles disassembled in multiple subunits with final height of less than 10 nm in average.

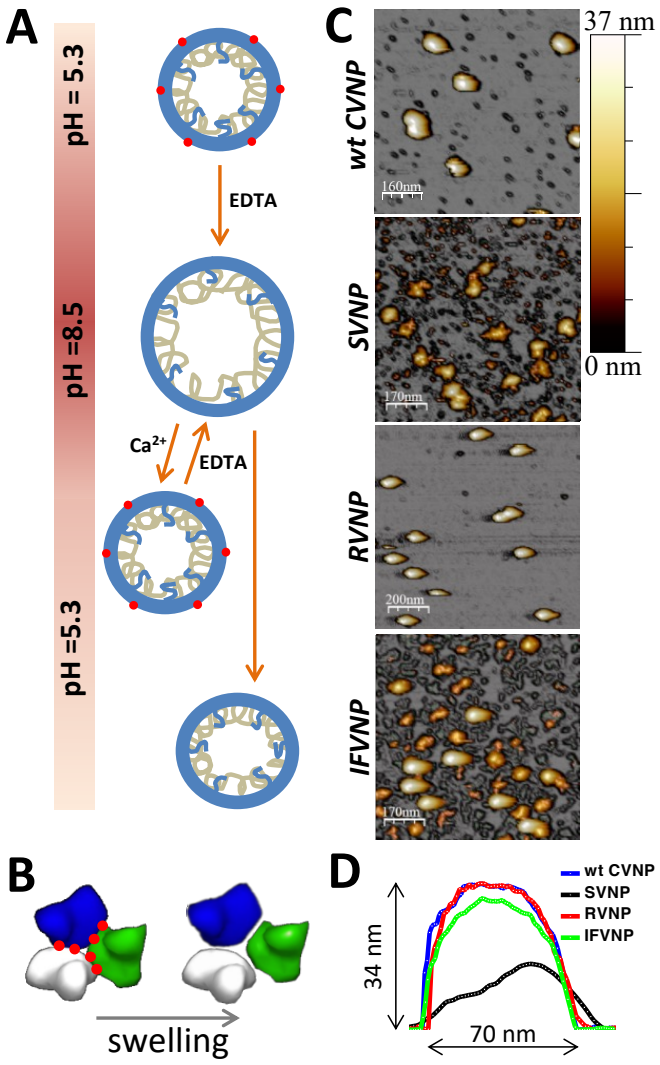
A
pH = 5.3
pH =8.5
pH =5.3
EDTA
Ca2+
EDTA
C
wt CVNP
SVNP
RVNP
IFVNP
37 nm
0 nm
160nm
170nm
200nm
170nm
B
swelling
D
wt CVNP
SVNP
RVNP
IFVNP
34 nm
70 nm
E
wt CVNPs
SVNPs
RVNPs
IFVNPs
# of particles
height (nm)

Figure 2. Schematic representation of the swelling process and height histogram of the adsorbed VNPs (A) Representation of the pH-induced expanding-compacting process. Under neutral conditions (pH=5.3) the Ca^{2+} ions are located at specific binding sites (red dots) contributing with an attractive component to the inter-protein interaction. The swelling of the particle was achieved by increasing the pH in the presence of EDTA. [22, 23, 30] This procedure promotes the expansion of the capsid as a consequence of the deprotonation of the aspartate residues at the calcium binding sites and the subsequent sequestration of such ions. The swollen forms were either (1) recompacted by lowering the pH in the presence of calcium (RVNPs) or (2) compacted by lowering the pH without calcium ions (IFVNPs). (B) Sketch of the conformational change associated with the swelling process. On the left, the subunits of the trimmer before the expansion are tightly packed and the Ca^{2+}-binding sites include the ions (red dots). On the right, after the expansion, the Ca^{2+} ions have been removed and the electrostatic repulsion between subunits opens pores at the quasi-threefold axes. (C) JM-AFM images, acquired in swelling buffer (pH=8.5) for SVNPs and in imaging buffer conditions (pH=5.3) for the rest of TBSV-NPs, show the adsorption of the different forms of TBSV-NPs. In this case, the areas scanned were about 800^2 nm^2. (D) Profiles of the different forms of TBSV-NPs absorbed on mica in liquid environment, taken along the central part of each particles. (E) Histograms of height of the different forms adsorbed on mica.

3.2. Mechanical properties. Nanoindentation experiments relied on squeezing individual VNPs with an AFM tip while registering the cantilever deflection *vs.* the piezo displacement [3] The resulting FICs (obtained after subtracting the deflection of the cantilever) provide information of the mechanical properties of the particle such as the stiffness and the elastic

limit. [4, 31] In addition to them, also resistance to material fatigue can be addressed by applying cyclic loading with single indentation assays.[10] Figure 3 shows, respectively, the mechanical and topographical evolution of a wt CVNP and a IFVNP. The consecutive FICs performed on the wt CVNP present three different mechanical responses: an elastic regime, an elastic-plastic regime, and a non-linear regime. FIC#1 (elastic regime) responds linearly until a force of about 4.8 nN, where a sharp drop of the force is registered. The small shoulder transition at a force of about 1.5 nN observed in this curve is likely caused by an adjustment of the AFM tip on the VNP surface (or of the VNP on the substrate), which explain why the slope of the FIC after this transition is maintained. In addition, the drop after the elastic limit, with a negative slope, indicates that the particle yields under the tip.[32] This feature suggests that the particle has likely suffered a structural damaged. The fact that the consecutive AFM images do not show a clear defect on the structure may be the consequence of a limitation on resolution; we need to keep in mind that the relative size of the tip-sample is almost 1. However, the retraction curve (blue line) supports the formation of a crack as the hysteresis loop that it defines is characteristic of an irreversible deformation. In addition, subsequent curve FIC#2 also corroborate this idea because the elastic limit is reached at lower values (~ 2 nN) and is followed by a smoother decrease in force, an indirect indicator of a change in the structure of the particle. From FIC#2 to FIC #6 the mechanical response of the particle shows an elastic-plastic regime. Finally, FIC#9 and FIC #10 do not longer present a linear regime at the beginning. The topographical control of the wt CVNP after each curve permits to monitor the gradual decrease in height after each indentation (Figures 3B and 3C) and evaluate the topography surface. Despite the change in the mechanical properties, AFM images show no any dismantlement of the viral shell until the tenth frame. Although the AFM

resolution does not allow to appreciate the cracks in the topography, it probes that TBSV-NPs are endorse with the ability of maintaining together their protein subunits into a round-shaped shell instead of dismantling. Likewise, Figure S4 confirms the absence of cracks and the progressive loss of height of three different wt CVNPs subjected to cyclic loading. On the other hand, the same experiment performed on an IFVNP (Figure 3D) does not reveal any difference between the FIC#1 and FIC#2. In this case, FIC#1 already displays a plastic transition at a similar force than in FIC#2. The topographical evolution of this particle also reveals an irreversible decrease in height without cracks along the consecutive loading (Figures 3E and 3F).

Figure 3. Cyclic loading with single indentation assays. (A) Cyclic loading performed on a wt CVNP. The red arrow show the upper limit of the fitting considered to calculate the

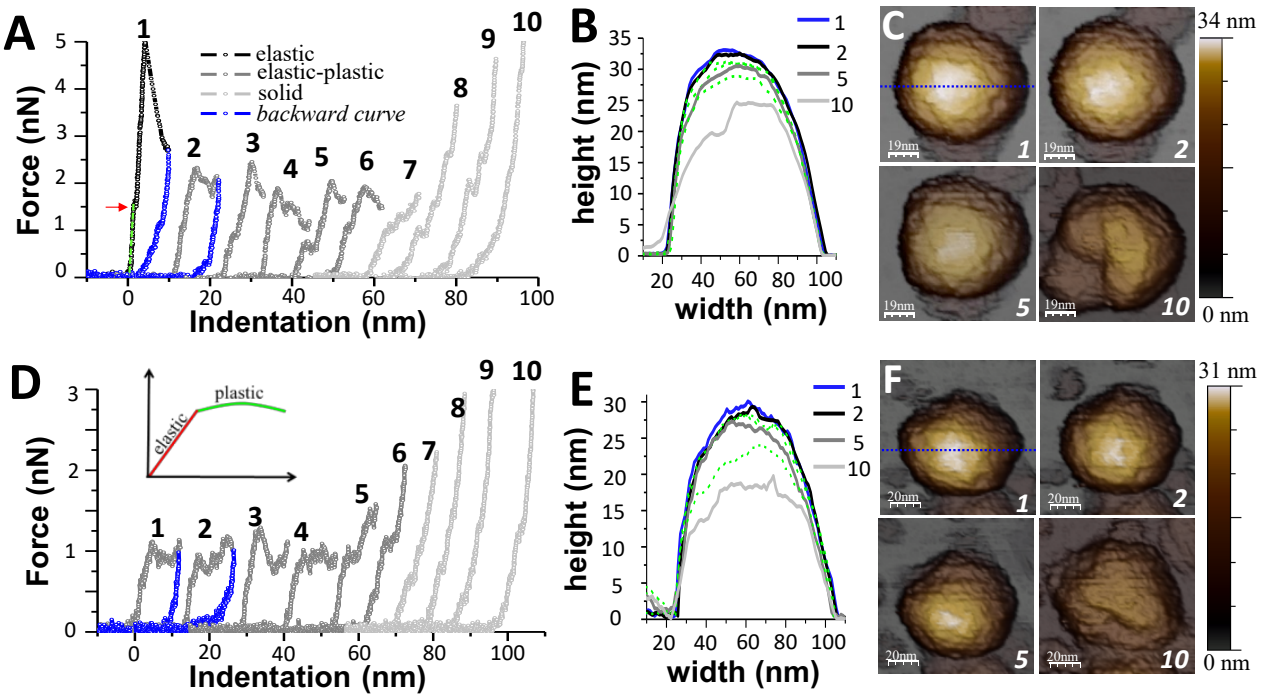

elastic constant (green dashed line) (B, C) Profile and topographic evolution of the wt CVNP along the consecutive loading. Profiles were taken on top of the VNP structures (marked with

a dotted blue line in the AFM images) and are labeled according to the number of FIC performed on it (i.e., the profile labeled as 1 shows the topography in which the FIC-1 was performed). (D, E, F) The same experiment performed on a IFVNP. The inset of Figure 3D illustrates the characteristic mechanical response of malleable material, consisting of an initial elastic response (red line) preceding a plastic deformation (blue line). All the images were acquired in JM-AFM under acidic buffer conditions (pH=5.3).

Figures 4A and 4B show the initial 3 FICs performed on 11 wt CVNPs and 16 IFVNPs, respectively. The comparison of the elastic limit along the loading cycles (Figure 4C) demonstrates that wt CVNPs and IFVNPs present a distinct behavior at the beginning (FIC#1) but similar in the subsequent deformations (FIC#2 and FIC#3). Likewise, Figure 4D depicts the evolution of the spring constant of the wt CVNPs (black line) and the IFVNPs (blue line). Although the stiffness decreases monotonically for both kinds of particles, wt CVNPs starts with a stiffer elastic constant. In addition, our data show that the FLAG chimera VNPs presented very similar mechanical parameters to those of the wt CVNPs (Table 1 in Supporting Information and Figure S4).

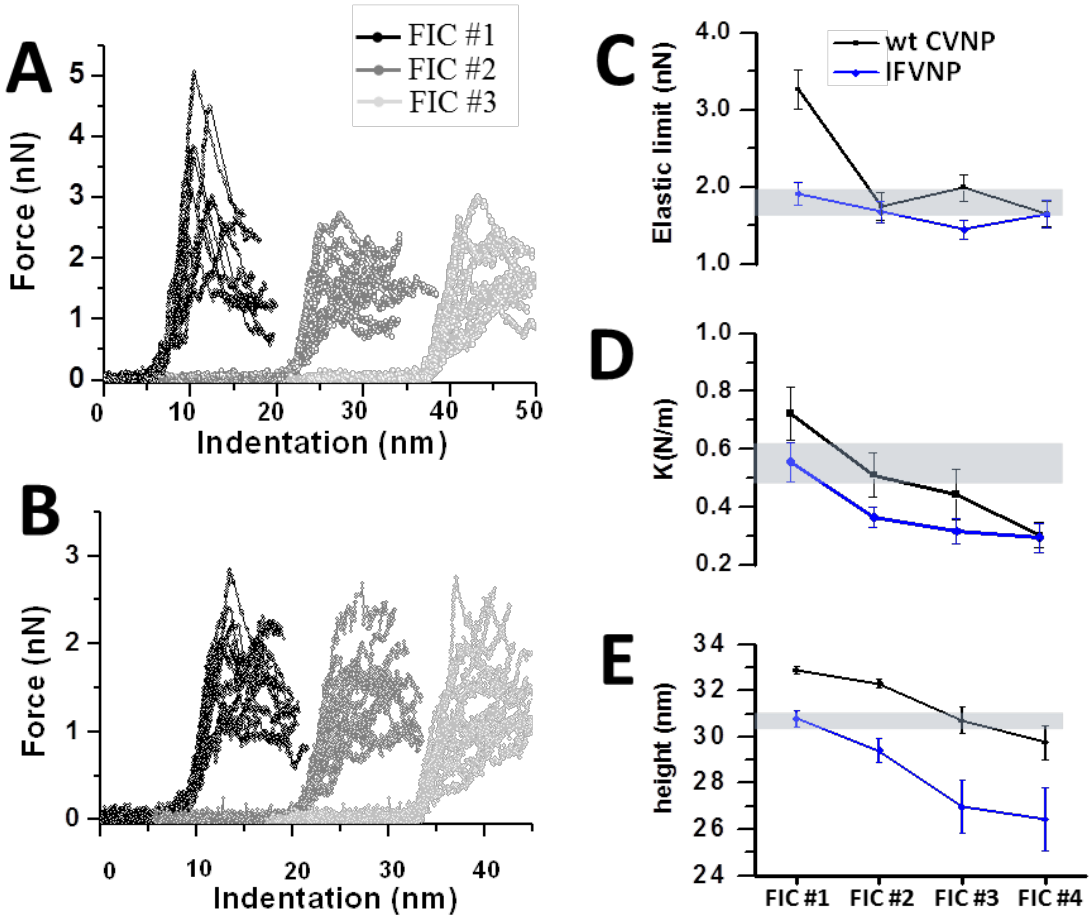

Figure 4. Comparison between the mechanical properties of wt CVNP and IFVNPs. (A) The graph shows the overlap of the first three FICs performed on 11 different wt CVNPs: first curve (black), second curve (dark grey), and third curve (light grey). (B) In this case the graphs show the curves performed on 15 IFVNPs. (C) Comparison of the evolution of the elastic limit between wt CVNPs (black line) and IFVNPs (blue line). (D) Comparison of the evolution of the elastic constant, obtained by fitting the linear part that precedes the plastic transition, for wt CVNPs (black line) and IFVNPs (blue line). (E) Comparison of the evolution of the height between wt CVNPs (black line) and IFVNPs (blue line). It indicates the average height of the particles before performing the corresponding FIC.

4. DISCUSSION

Presently, we discuss the results from a twofold perspective, including the topographical aspects of viral particles adsorption and the mechanical characterization addressed by nanoindentation experiments.

The high heterogeneity of charge density and hydrophobic patches within a virus shell permit the anchoring of the particle to substrates through a combination of van der Waals, electrostatic and hydrophobic forces. [33] Therefore, AFM imaging of absorbed particles provides valuable parameters that reveal subtle details about VNPs stability. Our experiments demonstrate that wt CVNPs and RCVNPs show a height (~34 nm) in agreement with the expected diameter of X-ray data, [24] probing the structural stability of these viruses upon absorption and demonstrating the reversibility of the swelling process. Contrariwise, the average height of IFVNPs (~29 nm) indicate that these structures were deformed about 15% in respect to their nominal size due to the force exerted by the surface. We also found that this reduction in height of IFVNPs was accompanied by a decrease in spring constant. This demonstrates that Ca^{2+} ions sequestration weakens the structure and increments the deformability of the particles, which results in a broader dispersion in height. On the other hand, the feeblest form of TBSV-NPs was found under alkaline conditions in the absence of Ca^{2+} ions, as the AFM images of SVNPs demonstrate, showing a deformation of about 70% (Figure 2C and S3). Since RVNPs were obtained from SVNPs by decreasing the pH in the presence of Ca^{2+} ions in solution, the collapse of SVNPs is likely caused by the interaction with the substrate. In addition, the geometry showed by the AFM images of SVNPs (Figures 2C and S2D) suggests that the internal RNA was likely ejected during the absorption as the

final size of the particles slightly corresponded to a wall-to-wall structure, similar to a deflated football.

The mechanical properties obtained in relation to the different kind of VNPs support the adsorption results afore discussed. If we consider the spring constant as a measurement of virus deformability, Figure 4D indicates that IFVNPs are softer than wt CVNPs in about 0.2 N/m. This major deformability could then explain why IFVNPs present a lower and more heterogeneous height. Indeed, the interaction between the IFVNPs and the surface may reduce the apparent height of the VNPs due to their major plasticity. The plastic behavior of TBSV-NPs is confirmed by the successive topographies obtained after each indentation which, after the monotonic decrease of the height (Figure 4E), do not show fractures or cracks of the viral shell (Figures 3C, 3F and S4). Previous mechanical studies of VNPs have shown that the AFM tip usually removes individual structural components. [10, 12, 15, 16] Most of times FICs presented a linear response that ended with a sudden drop of the force ascribed to the rupture of the structure. In contrast, our data show that FICs present a plastic regime that may be attributed to an irreversible deformation of the structure without fracture. The fact that TBSV-NPs do not present fracture under mechanical stress, [14] is likely caused by the presence of inner capsid protein tails that protrude into the virus interacting with the ssRNA and maintaining the viral subunits together. In fact, the last curves of the loading cycle for both particles reveal a Hertzian regime, typical of solids deformation. These final structures present a height which is compatible with the presence of RNA inside the viral particle. The complex amalgam of inner protein tails with the RNA genome likely flows plastically under mechanical stress avoiding the fracture of the structure into subunits.

Our results also suggest that the tendency to plasticity can be achieved by either deforming the particles with the AFM tip or by sequestering the calcium ions embedded into the capsid. Remarkably, we found that IFVNPs are mechanically indistinguishable from wt CVNPs that were previously squeezed: the second indentation performed on wt CVNPs shows that the stiffness of the particles decreases to the initial value of IFVNPs (Figure 4C). This analogy is further supported by the threshold of the plastic transition; while the first deformation of CVNPs present an elastic behavior until forces of about 3 nN, the successive FICs reach the plastic transition at the same values than IFVNPs (~1.7 nN) (Figure 4C). The differences between wt CVNPs and IFVNPs are likely the consequence of some unspecific inter-proteins rearrangements promoted by the chelation of calcium ions. The self-assembly process of TBSV-NPs needs a precise balance between electrostatic and entropic contributions of ions, capsid proteins and genome. [30] The lack of these calcium ions in the case of IFVNPs may likely introduce mismatches during the recompaction which promotes the softening of the VNPs and the decrease of their elastic limit. Nonetheless, structural studies have proved that the insertion of ions in the viral capsids increase their stability. [34] Therefore, by deforming the capsid with the AFM tip we may also induce some protein rearrangements that facilitate the plasticity of the capsids. The capacity of deforming plastically confers TBSV a great stability against fracture, and may be a sign of adaption for infecting plant cells. In fact, differently from animal viruses, plant viruses do not gain access into the cell by specific receptor-dependent internalization mechanisms but their entry is accompanied by a brute force necessary for damaging the cuticle and cell wall. [35]

Finally, we have studied the stability and mechanical response of TBSV-NPs whose outer surface was artificially modified. Functionalization by genetic modification of the coat

protein gene can be used to introduce new properties onto VNPs surface. In particular, using this approach a seven amino acid long spacer (GGPGGGG) followed by a eight amino acid long FLAG sequence (DYKDDDK) has been previously fused at the C-terminal end of the CP, known to be exposed and freely accessible on the outside of the TBSV-NPs, resulting on a stable display on each of the 180 CP subunits. [19] Our results demonstrate that this modification, which involves the whole external surface, does not alter the mechanical stability of the TBSV-NPs, which proves the robustness of these nanocages for future applications.

5. CONCLUSIONS

In this paper, we report the first experimental evidence of an elastic-plastic transition of individual viral cages. Specifically, we have subjected individual TBSV-NPs to consecutive loading cycles and have complementary compared the curves of deformation with the AFM images. The topographical characterization after each deformation has revealed the progressive and irreversible deformation of the capsid without cracks. We have also shown that Ca^{2+} ions are likely the molecular determinants of the elastic-plastic transition, since their depletion from the virus structure induce a decrease of the elastic limit. Our experiments demonstrate that this transformation can also be induced by squeezing the particles with the AFM tip, thus establishing a direct link between a chemical and a mechanical stresses. As TBSV-NPs are subjected to a brute force when entering the cell, they have to mechanically damage the cuticle and cell wall, [35] this parallelism could even find similarities during the plant cell infection. In any case, beyond its potential role during plant cell infection, plasticity

endow potential protein shells nanocontainer with extra structural stability as they are able to maintain the cargo constrained into the capsid under mechanical stress.

Acknowledgments

The authors of this paper would like to thank the MINECO of Spain (PIB2010US-0023,FIS2011-29493, Consolider CSD2010-00024, and CAM project nº.S2009/MAT-1467) for the financial support of this research. E.C. acknowledges a Short-Term Scientific Mission (STSM) supported by the COST Action TD 1002 AFM4NanoMed&Bio.

REFERENCES

1. Flint, S. J.; Enquist, L. W.; Racaniello, V. R.; Skalka, A. M., *Principles of virology*. ASM Press: Washington D.C., 2004.

2. Douglas, T.; Young, M., Host-guest encapsulation of materials by assembled virus protein cages. *Nature* 1998, 393, 152-155.

3. Ivanovska, I. L.; de Pablo, P. J.; Ibarra, B.; Sgalari, G.; MacKintosh, F. C.; Carrascosa, J. L.; Schmidt, C. F.; Wuite, G. J. L., Bacteriophage capsids: Tough nanoshells with complex elastic properties. *Proc. Natl. Acad. Sci. U. S. A.* 2004, 101, 7600-7605.

4. Carrasco, C.; Carreira, A.; Schaap, I. A. T.; Serena, P. A.; Gomez-Herrero, J.; Mateu, M. G.; de Pablo, P. J., DNA-mediated anisotropic mechanical reinforcement of a virus. *Proc. Natl. Acad. Sci. U. S. A.* 2006, 103, 13706-13711.

5. Hernando-Pérez, M.; Miranda, R.; Aznar, M.; Carrascosa, J. L.; Schaap, I. A. T.; Reguera, D.; de Pablo, P. J., Direct Measurement of Phage phi29 Stiffness Provides Evidence of Internal Pressure. *Small* 2012, 8, 2365.

6. Carrasco, C.; Castellanos, M.; de Pablo, P. J.; Mateu, M. G., Manipulation of the mechanical properties of a virus by protein engineering. *Proc. Natl. Acad. Sci. U. S. A.* 2008, 105, 4150-4155.

7. Castellanos, M.; Perez, R.; Carrasco, C.; Hernando-Perez, M.; Gomez-Herrero, J.; de Pablo, P. J.; Mateu, M. G., Mechanical elasticity as a physical signature of conformational dynamics in a virus particle. *Proc. Natl. Acad. Sci. U. S. A.* 2012, 109, 12028-12033.

8. Ortega-Esteban, A.; Pérez-Berná, A. J.; Menéndez-Conejero, R.; Gómez-Herrero, J.; Flint, S. J. C.; San Martín, C.; de Pablo, P. J., Monitoring disassembly of individual adenovirus particles shows stepwise dismantling and core uncoating in real time. *Scientific Reports* 2013, 3, 1434.

9. Roos, W. H.; Gertsman, I.; May, E. R.; Brooks, C. L.; Johnson, J. E.; Wuite, G. J. L., Mechanics of bacteriophage maturation. *Proc. Natl. Acad. Sci. U. S. A.* 2012, 109, 2342-2347.

10. Hernando-Pérez, M., E. Pascual, M. Aznar, A. Ionel, J. R. Castón, A. Luque, J. L. Carrascosa, D. Reguera, and P. J. de Pablo., The interplay between mechanics and stability of viral cages. *Nanoscale* 2014, 6, 2702-2709.

11. Cuellar, J. L.; Meinhoevel, F.; Hoehne, M.; Donath, E., Size and mechanical stability of norovirus capsids depend on pH: a nanoindentation study. *J. Gen. Virol.* 2010, 91, 2449-2456.

12. Snijder, J.; Uetrecht, C.; Rose, R. J.; Sanchez-Eugenia, R.; Marti, G. A.; Agirre, J.; Guerin, D. M. A.; Wuite, G. J. L.; Heck, A. J. R.; Roos, W. H., Probing the biophysical interplay between a viral genome and its capsid. *Nature Chemistry* 2013, 5, 502-509.

13. Carrasco, C.; Douas, M.; Miranda, R.; Castellanos, M.; Serena, P. A.; Carrascosa, J. L.; Mateu, M. G.; Marques, M. I.; de Pablo, P. J., The capillarity of nanometric water menisci confined inside closed-geometry viral cages. *Proc. Natl. Acad. Sci. U. S. A.* 2009, 106, 5475-5480.

14. Roos, W. H.; Bruinsma, R.; Wuite, G. J. L., Physical virology. *Nature Physics* 2010, 6, 733-743.

15. Ivanovska, I. L.; Miranda, R.; Carrascosa, J. L.; Wuite, G. J. L.; Schmidt, C. F., Discrete fracture patterns of virus shells reveal mechanical building blocks. *Proc. Natl. Acad. Sci. U. S. A.* 2011, 108, 12611-12616.

16. Castellanos, M.; Perez, R.; Carrillo, P. J. P.; de Pablo, P. J.; Mateu, M. G., Mechanical Disassembly of Single Virus Particles Reveals Kinetic Intermediates Predicted by Theory. *Biophys. J.* 2012, 102, 2615-2624.

17. Rapaport, D. C., Role of Reversibility in Viral Capsid Growth: A Paradigm for Self-Assembly. *Physical Review Letters* 2008, 101, 186101.

18. Young, M.; Willits, D.; Uchida, M.; Douglas, T., Plant Viruses as Biotemplates for Materials and Theri Use in Nanotechnology. *Annual Review of Phytpathology* 2008, 46, 361-384.

19. Grasso, S.; Lico, C.; Imperatori, F.; Santi, L., A plant derived multifunctional tool for nanobiotechnology based on Tomato bushy stunt virus. *Transgenic Resarch* 2012, 22, 519-35.

20. Luders, A.; Muller, C.; Boonrod, K.; Krczal, G.; Ziegler, C., Tomato bushy stunt viruses (TBSV) in nanotechnology investigated by scanning force and scanning electron microscopy. *Colloids and Surfaces B-Biointerfaces* 2012, 91, 154-161.

21. Olson, A. J.; Bricogne, G.; Harrison, S. C., Structure of Tomato Bushy Stunt Virus .4. The Virus Particle at 2.9 a Resolution. *J. Mol. Biol.* 1983, 171, 61-93.

22. Robinson, I. K.; Harrison, S. C., Structure of the Expanded State of Tomato Bushy Stunt Virus. *Nature* 1982, 297, 563-568.

23. Kruse, J.; Kruse, K. M.; Witz, J.; Chauvin, C.; Jacrot, B.; Tardieu, A., Divalent Ion-Dependent Reversible Swelling of Tomato Bushy Stunt Virus and Organization of the Expanded Virion. *J. Mol. Biol.* 1982, 162, 393-414.

24. Hopper, P.; Harrison, S. C.; Sauer, R. T., Structure of Tomato Bushy Stunt Virus .5. Coat Protein-Sequence Determination and Its Structural Implications. *J. Mol. Biol.* 1984, 177, 701-713.

25. Ortega-Esteban, A.; Horcas, I.; Hernando-Perez, M.; Ares, P.; Perez-Berna, A. J.; San Martin, C.; Carrascosa, J. L.; de Pablo, P. J.; Gomez-Herrero, J., Minimizing tip-sample forces in jumping mode atomic force microscopy in liquid. *Ultramicroscopy* 2012, 114, 56-61.

26. Butt, H. J., Electrostatic Interaction in Atomic Force Microscopy. *Biophys. J.* 1991, 60, 777-785.

27. Sotres, J.; Baro, A. M., AFM Imaging and Analysis of Electrostatic Double Layer Forces on Single DNA Molecules. *Biophys. J.* 2010, 98, 1995-2004.

28. Mateu, M. G., *Structure and Physics of Viruses*. Springer: London, 2013; Vol. 68.

29. Horcas, I.; Fernandez, R.; Gomez-Rodriguez, J. M.; Colchero, J.; Gomez-Herrero, J.; Baro, A. M., WSXM: A software for scanning probe microscopy and a tool for nanotechnology. *Rev. Sci. Instrum.* 2007, 78, 013705.

30. Aramayo, R.; Merigoux, C.; Larquet, E.; Bron, P.; Perez, J.; Dumas, C.; Vachette, P.; Boisset, N., Divalent ion-dependent swelling of tomato bushy stunt virus: A multi-approach study. *Biochimica Et Biophysica Acta-General Subjects* 2005, 1724, 345-354.

31. Michel, J. P.; Ivanovska, I. L.; Gibbons, M. M.; Klug, W. S.; Knobler, C. M.; Wuite, G. J. L.; Schmidt, C. F., Nanoindentation studies of full and empty viral capsids and the effects of capsid protein mutations on elasticity and strength. *Proc. Natl. Acad. Sci. U. S. A.* 2006, 103.

32. Perez-Berna, A. J.; Ortega-Esteban, A.; Menendez-Conejero, R.; Winkler, D. C.; Menendez, M.; Steven, A. C.; Flint, S. J.; de Pablo, P. J.; San Martin, C., The Role of Capsid Maturation on Adenovirus Priming for Sequential Uncoating. *J. Biol. Chem.* 2012, 287, 31582-31595.

33. Muller, D. J.; Amrein, M.; Engel, A., Adsorption of biological molecules to a solid support for scanning probe microscopy. *J. Struct. Biol.* 1997, 119, 172-188.

34. Erk, I.; Huet, J. C.; Duarte, M.; Duquerroy, S.; Rey, F.; Cohen, J.; Lepault, J., A zinc ion controls assembly and stability of the major capsid protein of rotavirus. *J. Virol.* 2003, 77, 3595-3601.

35. Shaw, J. G., Tobacco mosaic virus and the study of early events in virus infections. *Philosophical Transactions of the Royal Society of London Series B-Biological Sciences* 1999, 354, 603-611.